The Predictive Power of Computational Astrophysics as a Discovery Tool
Proceedings IAU Symposium No. 362, 2023
D. Bisikalo, D. Wiebe & C. Boily, eds.
doi:10.1017/S1743921322001624

X-ray spectral and image spatial models of NGC 3081 with *Chandra* data

O.V. Kompaniiets[1,2], Iu.V. Babyk[1], A.A. Vasylenko[1], I.O. Izviekova[1,3] and I.B. Vavilova[1]

[1]Main Astronomical Observatory of the NAS of Ukraine, 27 Akademik Zabolotny Str., Kyiv, 03143, Ukraine

[2]Institute of Physics of the NAS of Ukraine, 46 av. Nauky, Kyiv, 03028, Ukraine

[3]ICAMER, NAS of Ukraine, 27 Akademik Zabolotny Str., Kyiv, 03143, Ukraine

Abstract. The physical properties of AGN such as accretion rate, column density, temperature of hot corona and other characteristics can be found from X-ray spectral data. We present the results of spatial and spectral analysis for Sy2 type galaxy NGC 3081 obtained with different mathematical tools of the Chandra Interactive Analysis of Observations software. We found evidence of extended emission in 0.5-3.0 keV as well as derived parameters for model A: photon index $\Gamma = 1.65^{+0.1}_{-0.9}$, column density $N_H = 57.5^{+5.7}_{-2.8} cm^{-2}$, warm component $kT_1 = 0.16^{+0.1}_{-0.02}$ and hot component $kT_2 = 1.0^{+3.0}_{-0.1}$ keV. We detected the presence of a component of the reflection spectrum, Fe K_α emission line with $E_{line} = 6.39^{+0.06}_{-0.02}$keV and $EW = 50^{+0.01}_{-0.01}$ eV.

Keywords. methods: data analysis – galaxies: active galactic nuclei – NGC 3081

1. Introduction

Active galactic nuclei (AGNs) are one of the most powerful sources in the Universe. The main parts of the AGNs, such as an accretion disc, a torus, and a supermassive black hole (SMBH), testify themselves by different kinds of radiation (see, the Unification Scheme by Antonucci & Miller (1985)). The optical and UV emission from AGN arises due to the accretion process onto the SMBH, while the X-ray emission originates by Compton upscattering of optical/UV photons from the hot corona (Haardt & Maracchi 1991, 1993). This X-ray radiation is typically described by a power-law model and an exponential cut-off at high energies. In addition to these components of spectra there are a reflection spectrum appearing as a "reflection hump" at $\sim 20 - 30$ keV and a Fe K_α line near 6.4 keV (Mushotzky et al. (1993); Ramos & Ricci (2017); Kompaniiets & Vasylenko (2020)).

The AGN's drive is fueled and evolved by both intrinsic processes and environmental influence. To distinguish these factors, we propose considering isolated galaxies with AGNs, which had not undergone tidal effects during at least 3 Gyrs. Our sample of 61 isolated AGNs was formed by cross-matching the 2MIG (2MASS Isolated Galaxy) catalogue with the Veron-Cetty catalogue of quasars and AGNs, where the restriction was used for $K_s \leq 12.0$ mag and $V_r < 15\,000$ km/s (Pulatova et al. (2015); Karachentseva et al. (2010); Véron-Cetty & Véron (2010). They belong to the Local Universe and are located not in dense regions, like Virgo and Fornax clusters or galaxy groups of the Local Supercluster (Karachentseva & Vavilova (1994); Karachentseva & Vavilova (1995); Vavilova et al. (2005)). For the first time, we revealed that the host isolated galaxies with AGNs of Sy1 type (without faint companions) appear to possess the bar morphological features, which

provide transfer of gas and dust from galaxy's disc to AGN region (Pulatova et al. 2015) Therefore, the interaction with neighbouring galaxies is not a necessary condition for BLR formation in comparison with dual AGNs triggered by tidally induced gas inflows (Smirnova et al. (2010); Gross et al. (2019); Guainazzi et al. (2021)). Withal, the isolated AGN and AGNs in pairs (or mergers) show similar distributions in their global stellar mass, star-formation rate, and central [O III] surface brightness (Jin et al. (2021)).

We performed the X-ray spectral analysis for isolated AGNs with the XMM-Newton, Chandra, and Swift/XRT data in their computational software (Vavilova et al. (2015); Vasylenko (2020). It allowed revealing that isolated AGNs mostly have smaller luminosity $L_{2-10keV} \sim 10^{42}$ erg/s in comparison with the typical luminosity for the Seyfert galaxies (see, for example, Volvach et al. (2011). The spectra of NGC 5347 and MCG-02-09-040 show the neutral Fe K_α emission line. The X-ray spectrum of NGC 5347 is described by a pure reflection model with $E_{cut} \sim 117$ keV and with no signs of transmitted radiation, while MCG-02-09-040 shows the presence of heavy neutral obscuration of $N_H \sim 10^{24}$ cm^{-2}.

In this work, we present the results of the X-ray spectral analysis of yet another low-luminosity isolated S0/a galaxy NGC 3081 with Sy2 nucleus based on the Chandra data. It's worth noting that NGC 3081 has a complicated structure: a weak large scale bar and a nuclear bar, and four resonance rings - two outer rings, an inner ring, and a nuclear ring (Schnorr-Müller et al. (2016)).

2. X-ray spectral analysis of NGC 3081

The software for Chandra X-ray observatory called **CIAO** is available through (`https://cxc.cfa.harvard.edu/ciao/`). Observations of NGC 3081 were done in 2018 (OBSID 20622) with a total exposure 22.3 ks. We reprocessed these data by standard script called `chandra_repro`. Spectrum was extracted by `specextract` tool with radius 1.6783″. The background spectrum was created for annulus with the radii $R_1 = 4.873''$ and $R_2 = 9.743''$ and centered for the source region. To take into account telescope response we created the Auxiliary Response Files and the Redistribution Matrix Files. To apply χ^2 statistics the spectrum was grouped with `group_counts` with a 20 counts per been (Fig. 1). Finally, the spectrum was constructed by CIAO modeling and fitting application called `Sherpa` (Freeman et al. 2001; Doe et al. 2007).

A simple phenomenological model (model A) in `Sherpa` terminology is as follows:

```
Model A = xstbabs × (xsapec + xsapec + xsztbabs × xszpowerlw + xszgauss)
```

It includes power-law continuum (`xszpowerlaw`), neutral absorption (`xsztbabs`), emission line with a Gaussian profile (`xszgauss`), and two thermal components (`xsapec`). Galactic absorption was fixed with value $N_H = 0.04 \cdot 10^{22} cm^{-2}$.

We obtained photon index $\Gamma = 1.65^{+0.1}_{-0.9}$, and column density is $N_H = 57.5^{+5.7}_{-2.8}\ cm^{-2}$. Two different thermal components were also detected: a warm one with temperature $kT_1 = 0.16^{+0.10}_{-0.02}$ and a hot one with temperature $kT_2 = 1.0^{+3.0}_{-0.1}$ keV. The Fe K_α emission line is $E_{line} = 6.39^{+0.06}_{-0.02}$keV and equivalent width is $EW = 50^{+0.01}_{-0.01}$ eV. It's suggested that the Fe K_α emission line is originated in moderate density environment.

3. Image spatial analysis of NGC 3081

The Chandra telescope has the best angular resolution among all the X-ray space observatories (0.492 arcsec). This makes possible to use its observational data for spatial analysis too. The point spread function (PSF) describes the shape and size of the image produced by a delta function (a point) source. The shape and size of the High-Resolution

https://doi.org/10.1017/S1743921322001624 Published online by Cambridge University Press

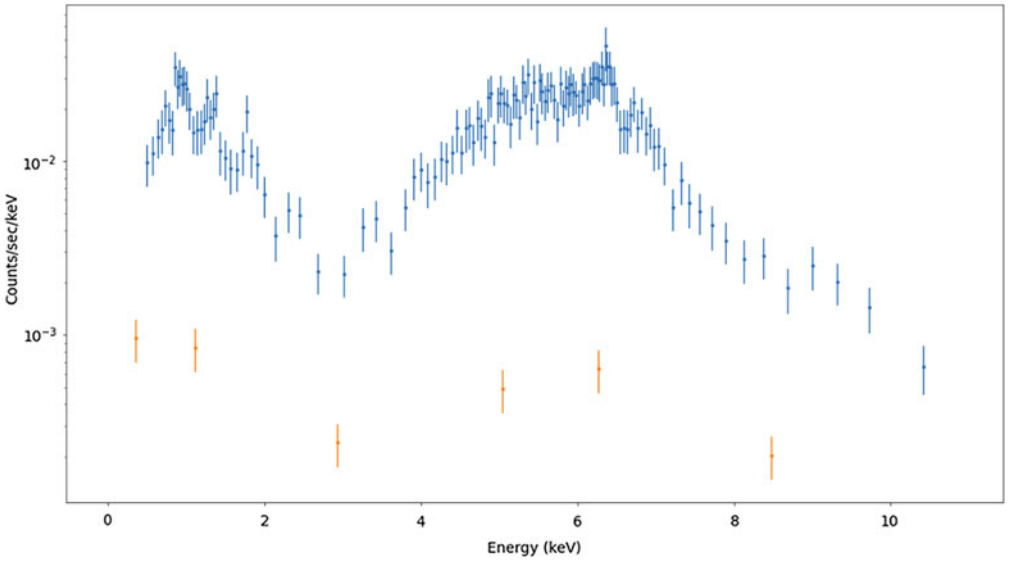

Figure 1. The source and background spectrum for NGC 3081 with Chandra software.

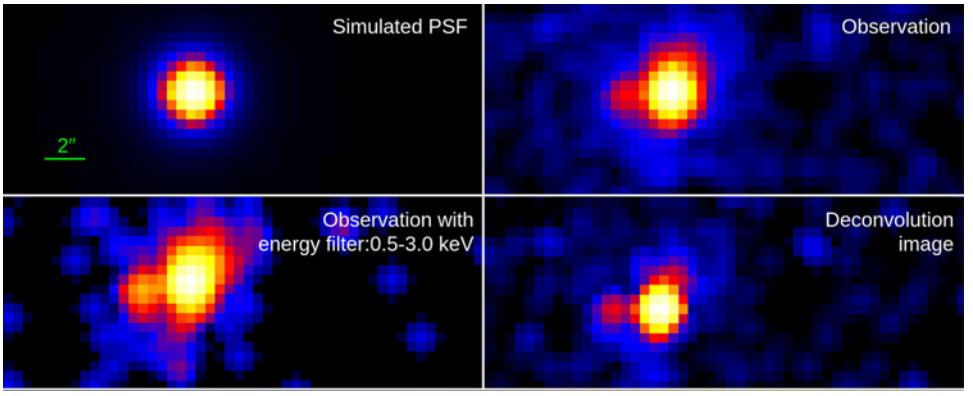

Figure 2. Image spatial analysis of NGC 3081. Top left panel: the MARX simulated PSF, top right panel: observable image, left down panel: observable image with energy filter 0.5-3.0 keV, right down panel: deconvolved image with bin size 4923″.

Mirror Assembly (HRMA) PSF vary significantly with source location in the telescope field of view and spectral energy distribution. The PSF should be simulated with **MARX**, where the input spectrum is created with a baseline model (for example, power-law and absorption). Parameters for this model were estimated from a simple fit for the source spectrum. The next step after the PSF simulation is to restore image resolution. For this procedure, the Lucy-Richardson deconvolution algorithm is applied, which is implemented in the `arestore` tool. In the case of NGC 3081, we used results from Model A. The obtained PSF, observational and deconvolutional images are given in Fig. 2. These results were put on the sub-pixel image with 1/2 and 1/8 bin size of the Chandra ACIS instrument (Fig. 3).

4. Conclusion

We presented the results of X-ray spectral and spatial analysis for NGC 3081 based on the Chandra observational data and Chandra Interactive Analysis of Observations

https://doi.org/10.1017/S1743921322001624 Published online by Cambridge University Press

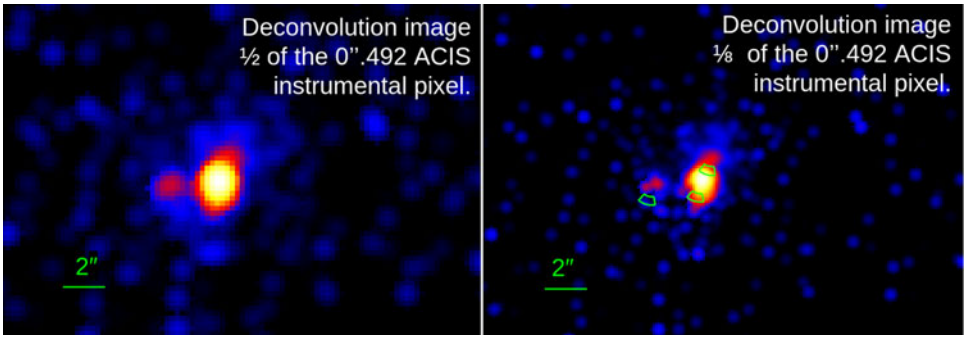

Figure 3. Image spatial analysis of NGC 3081. Left panel: sub-pixel deconvolved image with bin size 2463″. Right panel: sub-pixel deconvolved image with bin size 61.53″, where green regions characterise the HRMA artifact indicating that this part is not related to the source.

software. We found an evidence of extended emission in 0.5-3.0 keV and obtained parameters for model A: photon index $\Gamma = 1.65^{+0.1}_{-0.9}$, column density $N_H = 57.5^{+5.7}_{-2.8} cm^{-2}$, warm component with $kT_1 = 0.16^{+0.1}_{-0.02}$ and hot component with $kT_2 = 1.0^{+3.0}_{-0.1}$ keV. We detected the presence of one of the components of the reflection spectrum such as Fe K_α emission line with $E_{line} = 6.39^{+0.06}_{-0.02}$keV and $EW = 50^{+0.01}_{-0.01}$ eV.

Acknowledgements

This work has used data obtained from the Chandra Data Archive and the Chandra Source Catalog, and software provided by the Chandra X-ray Center (CXC) in the application packages CIAO and Sherpa. The authors note the support of the Grant for young research laboratories of the NAS of Ukraine (No07/01-2021(3)).

References

Antonucci R., Miller J. 1985, *ApJ*, 297, 621
Chesnok N.G., Sergeev S.G., Vavilova I.B. 2009, *Kinemat. Physics Celest. Bodies*, 25, 107.
Doe S., Nguyen D., Stawarz C. et al. 2007, *ADASS XVI*, 376, 543.
Freeman P., Doe S., Siemiginowska A. 2001, *Astronomical Data Analysis*, 4477, 76.
Gross A. et al. 2019, *AAS Meeting Abstracts*, #233.
Guainazzi M., De Rosa A., Bianchi S. et al. 2021, *MNRAS*, 504, 393.
Haardt F., Maraschi L. 1991, *ApJ*, 380, 51
Haardt F., Maraschi L. 1993, *ApJ*, 413, 507
Jin G., Dai Y.S., Pan H.A. et al. 2021, *Astrophys. J.*, 923, 6.
Karachentseva V.E. and Vavilova I.B. 1994, *Bull.Special Astrophys. Observatory* 37, 98.
Karachentseva V.E. and Vavilova I.B. 1995, *Kinemat. Phys. Celestial Bodies* 11, 38.
Karachentseva V.E., Mitronova S.N., Melnyk O.V. et al 2010, *Astrophys. Bull.*, 65, 1.
Kompaniiets O.V. & Vasylenko A.A. 2020, *Astrophysics*, 63, 307.
Mushotzky R.F., Done C., Pounds K.A. 1993 *A*nnual Rev. Astron. Astrophys.31, 717
Pulatova N.G., Vavilova I.B., Sawangwit U., et al. 2015, *Mon. Not. R. Astron. Soc.*, 447, 3, 2209.
Ramos A.C. & Ricci C. 2017, *Nature Astronomy*, 1, 679.
Schnorr-Müller A. et al. 2016, *MNRAS*, 457, 972.
Smirnova A.A., Moiseev A.V., Afanasiev V.L. 2010, *Hunting for the Dark: the Hidden Side of Galaxy Formation*, 1240, 297.
Vasylenko A.A., Vavilova I.B., Pulatova N.G. 2020, *Astron. Nachr.*, 341, 8, 801.

https://doi.org/10.1017/S1743921322001624 Published online by Cambridge University Press

Vavilova I.B., Karachentseva V.E., Makarov D.I., and Melnyk O.V. 2005, *Kinemat. Fiz. Nebesnykh Tel* 21, 3.
Vavilova I.B., Vasylenko A.A., Babyk Iu.V., Pulatova N.G. 2015, *Odessa Astron. Publ.*, 28(2), 150.
Véron-Cetty M.P., Véron P. 2010, *Astron. Astrophys.*, 518, A10.
Vol'Vach, A.E., Vol'Vach L.N., Kut'kin A.M. et al. 2011, *Astron. Reports* 55, 608.